



Biotin-targeted Pluronic[®] P123/F127 mixed micelles delivering niclosamide: A repositioning strategy to treat drug-resistant lung cancer cells



Annapina Russo^{a,1}, Diogo Silva Pellosi^{b,c,1}, Valentina Pagliara^a, Maria Rita Milone^d, Biagio Pucci^d, Wilker Caetano^c, Noboru Hioka^c, Alfredo Budillon^d, Francesca Ungaro^{b,*}, Giulia Russo^{a,*}, Fabiana Quaglia^b

^a Laboratory of Biochemistry, Department of Pharmacy, University of Napoli Federico II, Via Domenico Montesano 49, 80131 Napoli, Italy

^b Laboratory of Drug Delivery, Department of Pharmacy, University of Napoli Federico II, Via Domenico Montesano 49, 80131 Napoli, Italy

^c Research Nucleus of Photodynamic Therapy, Chemistry Department State University of Maringá, Av. Colombo 5.790, 87020-900, Maringá, Paraná, Brazil

^d Experimental Pharmacology Unit, Department of Research, Istituto Nazionale Tumori-IRCCS G. Pascale Via M. Semmola, 80131 Napoli, Italy

ARTICLE INFO

Article history:

Received 6 June 2016

Received in revised form 24 June 2016

Accepted 26 June 2016

Available online 29 June 2016

Keywords:

Micelle

Pluronic[®]

Niclosamide

Lung cancer cells

Multidrug resistance

ABSTRACT

With the aim to develop alternative therapeutic tools for the treatment of resistant cancers, here we propose targeted Pluronic[®] P123/F127 mixed micelles (PMM) delivering niclosamide (NCL) as a repositioning strategy to treat multidrug resistant non-small lung cancer cell lines. To build multifunctional PMM for targeting and imaging, Pluronic[®] F127 was conjugated with biotin, while Pluronic[®] P123 was fluorescently tagged with rhodamine B, in both cases at one of the two hydroxyl end groups. This design intended to avoid any interference of rhodamine B on biotin exposition on PMM surface, which is a key fundamental for cell trafficking studies. Biotin-decorated PMM were internalized more efficiently than non-targeted PMM in A549 lung cancer cells, while very low internalization was found in NH3T3 normal fibroblasts. Biotin-decorated PMM entrapped NCL with good efficiency, displayed sustained drug release in protein-rich media and improved cytotoxicity in A549 cells as compared to free NCL ($P < 0.01$). To go in depth into the actual therapeutic potential of NCL-loaded PMM, a cisplatin-resistant A549 lung cancer cell line (CPr-A549) was developed and its multidrug resistance tested against common chemotherapeutics. Free NCL was able to overcome chemoresistance showing cytotoxic effects in this cell line ascribable to nucleolar stress, which was associated to a significant increase of the ribosomal protein rpl3 and consequent up-regulation of p21. It is noteworthy that biotin-decorated PMM carrying NCL at low doses demonstrated a significantly higher cytotoxicity than free NCL in CPr-A549. These results point at NCL-based regimen with targeted PMM as a possible second-line chemotherapy for lung cancer showing cisplatin or multidrug resistance.

© 2016 Elsevier B.V. All rights reserved.

1. Introduction

Cancer is the leading cause of mortality worldwide and its incidence continues to rise (Siegel et al., 2015). Although the discovery of novel and effective anticancer drugs is a major research area, it is well known that the development of new chemotherapeutics in oncology is a lengthy and extremely costly process. Furthermore, it often results in only slight reduction of

chemotherapy-related side effects and minimal increase in the overall survival rate. Therefore, alternative approaches to anticancer drug discovery are needed.

To reduce pharmaceutical research costs and development timelines, considerable attention has been devoted to the so called drug “repositioning” or “repurposing” approach, which entails finding novel therapeutic indications for already approved drugs (Ashburn and Thor, 2004). Some successful repositioning stories, such as those of minoxidil, sildenafil and raloxifene, are very well known. Nevertheless, despite several initiatives, only a few drugs have been successfully approved for new indications (Novac, 2013). In recent years, this approach has been very promising to identify approved non-cancer drugs that possess anticancer

* Corresponding authors at: Department of Pharmacy, University of Napoli Federico II, Via Domenico Montesano 49, 80131 Napoli, Italy.

E-mail addresses: ungaro@unina.it (F. Ungaro), giulia.russo@unina.it (G. Russo).

¹ The authors equally contributed to this work.

activity, thus abbreviating the development process (Shim and Liu, 2014).

Some studies have reported the inhibitory effects of niclosamide (5-Chloro-*N*-(2-chloro-4-nitrophenyl)-2-hydroxybenzamide) (NCL), an anthelmintic drug approved for use in humans for nearly 50 years, on multiple intracellular signalling pathways (Balgı et al., 2009; Liu et al., 2015; Ren et al., 2010; Sack et al., 2011; Xiang et al., 2015). The signaling molecules in these pathways are either over-expressed, constitutively activated or mutated in many cancer cells, thus making NCL a very intriguing tool for cancer treatment (Li et al., 2014). Indeed, NCL inhibits the ATP-binding cassette efflux pump ABCG2 (breast cancer resistance protein or BCRP) (Strouse et al., 2013), which is a protein able to confer Multi Drug Resistance (MDR) to a broad spectrum of anticancer drugs (Staud and Pavék, 2005). Furthermore, NCL exhibits antitumor activity *in vitro* and *in vivo* by suppressing the expression of lipoprotein receptor-related protein (LRP), thus inhibiting Wnt/ β -catenin signaling in human prostate and breast tumor cells. LRP has been involved in the resistance of ovarian cancer cells to cisplatin and shown to play an important role in the transport of cisplatin (Wang et al., 2004).

The major concern related to the therapeutic use of NCL is its very low solubility and consequent poor dissolution properties in biological fluids. Furthermore, the bioaccessibility of systemic anticancer drugs to tumour tissue remains limited and large drug doses are commonly required to exert a therapeutic effect, with consequent high toxicity to normal cells and increased incidence of MDR.

Overwhelming attention is nowadays devoted to novel polymeric carriers with tailored properties to attain efficient transport of chemotherapeutics in the body (d'Angelo et al., 2014). Pluronic[®] polymers are amphiphilic triblock copolymers of poly(ethylene oxide) (PEO) and poly(propylene oxide) (PPO), which self-assemble in aqueous media forming core-shell micelles (Kabanov et al., 2002). Due to their ability to accommodate hydrophobic drugs in the PPO core, Pluronic[®] micelles have been proposed to solve solubility issues of several drugs (Alvarez-Lorenzo et al., 2011). Furthermore, Pluronic[®] micelles possess unique beneficial features for cancer therapy, that is: (i) small size (<100 nm) useful to prolong drug circulation time and to promote its passive targeting to solid tumors (Batrakova and Kabanov, 2008; Zhu et al., 2016); (ii) inhibition of drug efflux transporters overcoming MDR (Alakhova and Kabanov, 2014; Alvarez-Lorenzo et al., 2011); (iii) presence of hydroxyl end groups allowing the covalent binding of targeting ligands and imaging agents providing multifunctionality (Ding et al., 2011; Jung et al., 2013; Zhang et al., 2011).

Recently our group has developed Pluronic[®] P123/F127 mixed micelles that are stable in biologically-relevant media and able to load and stabilize hydrophobic benzoporphyrin derivatives for photodynamic therapy application (Pellosi et al., 2016). In analogy to all PEO-coated nanocarriers, Pluronic[®] micelles suffer poor uptake in cancer cells due to increased surface hydrophilicity, which can be a drawback when trying to accumulate drug cargo intracellularly. To overcome this issue, and hopefully improve therapeutic effects in a biological environment, surface decoration with small targeting ligands is a common strategy to encourage carrier accumulation in targeted cells (Stylianopoulos and Jain, 2015). The vitamin biotin, an essential micronutrient that could give tumor-targeting properties, has been recently proposed to this purpose. In fact, several cancer cell lines overexpress biotin-specific receptors such as avidin, neutravidin, and streptavidin that facilitate receptor-mediated endocytosis of biotinylated nanoparticles in cancer cells (Chen et al., 2010; Morral-Ruiz et al., 2015). To track micelles in a biological milieu, a fluorescent probe can be covalently linked to polymer unimers providing fluorescent

micelles. In fact, imaging-based techniques allow understanding of micelle dynamic, monitoring their body distribution and real-time cell uptake, thus bringing tremendous advantages in relating trafficking to biological effects (Wang et al., 2014).

With this idea in mind, here we have developed a multifunctional platform for the delivery of NCL to cancer cells comprising Pluronic[®] P123/F127 mixed micelles (PMM) surface-decorated with the vitamin biotin as targeting agent and further engineered with a fluorescent tag for cell imaging purposes. After formulation studies aimed at assessing the best conditions to entrap and release NCL, NCL-loaded biotin-decorated PMM have been obtained. The role played by biotin decoration on PMM selectivity toward lung cancer cells, and its consequent cytotoxicity in cells either sensitive or resistant to cisplatin, were elucidated. We generated and characterized a cisplatin-resistant non-small lung cancer cell line, providing a valuable tool for investigating both the therapeutic potential of NCL to overcome MDR in cancer cells and the mechanism through which the drug exerts its cytotoxic effect.

2. Materials and methods

2.1. Materials

Pluronic[®] P123 (EO₂₀-PO₆₅-EO₂₀, MW = 5750 g mol⁻¹) and F127 (EO₁₀₀-PO₆₅-EO₁₀₀, MW = 12600 g mol⁻¹), biotin, HABA/avidin reagent, *N,N'*-dicyclohexylcarbodiimide (DCC), 4-dimethylamino-pyridine (DMAP), niclosamide (NCL), rhodamine B and trehalose were obtained from Sigma-Aldrich (Italy). Ethanol, dichloromethane, diethyl ether, acetone and acetonitrile were purchased from Carlo Erba Reagents (Italy). Dimethyl sulfoxide-*d*₆ (DMSO-*d*₆), D₂O and all deuterated solvents for nuclear magnetic resonance (NMR) spectroscopy were purchased from Merck (Italy). All the other chemicals were of analytical reagent grade and used without previous purification.

2.2. Synthesis of biotin-conjugated and rhodamine-conjugated Pluronic[®]

The synthetic procedure was adapted from the literature (Li et al., 2010) and was similar for both P123 and F127. For biotin-conjugated Pluronic[®], F127 (5.0 g, 0.40 mmol) was dissolved in 75 mL of dichloromethane followed by the addition of biotin (0.12 g, 0.48 mmol). For Rhodamine-conjugated Pluronic[®], P123 (3.0 g, 0.40 mmol) was dissolved in 75 mL of dichloromethane followed by the addition of rhodamine B (0.44 g, 0.48 mmol). After that, DMAP (0.004 g, 0.03 mmol) was added to each reaction flask and the solution cooled to 0 °C. DCC (0.08 g, 0.40 mmol) was added dropwise *via* a dropping funnel over 30 min, and the reactions were carried out for 48 h at room temperature under stirring. The reaction mixtures were then extracted with a NaHCO₃ water solution (10% v/v). After this step, the organic phases were frozen overnight and the insoluble substances were removed by filtration. The organic solutions were then precipitated twice in cold diethyl ether. The functionalized polymers were filtered and dried overnight under vacuum.

Biotin-F127 reaction yield = 82%. ¹H NMR (300 MHz, DMSO-*d*₆, TMS), δ (ppm): 1.000–1.485 (s, -CH₃ b), 1.493 (m, H₅, 2H), 2.200 (m, H₃, 2H), 2.821 (m, H₅, 2H), 3.105 (m, H₄, 2H), 3.260–3.619 (m, -O-CH₂-CH₂-a), 4.138 (m, H₆, 1H), 4.300 (m, H₆, 1H), 6.363 (s, H_{N2}, 1H) e 6.437 (s, H_{N1}, 1H).

Rhodamine-P123 reaction yield = 68%. ¹H NMR (300 MHz, DMSO-*d*₆, TMS), δ (ppm): 1.000–1.126 (s, -CH₃ b), 1.209 (t, N-CH₃, 12H), 3.260–3.549 (m, -O-CH₂-CH₂-a), 3.641 (d, N-CH₂, 8H), 6.980 (m, H₂-H₇-H₄-H₅, 4H), 7.094 (d, H₈-H₁, 2H), 7.473 (dd, H₆, 1H), 7.842 (m, H₄'-H₅', 2H), 8.320 (dd, H₃', 1H).

2.3. Preparation of micelles

Unloaded and NCL-loaded Pluronic[®] mixed micelles (PMM) were prepared by thin-film hydration method (Zhang et al., 1996). Briefly, different amounts of a P123/F127 mixture (2:1 w/w) were dissolved in ethanol in a round-bottom flask to give solutions at different concentrations (10–50 mg mL⁻¹). For drug-loaded micelles, different amounts of NCL (0.1–1.0 mg mL⁻¹) were dissolved in ethanol and added to Pluronic[®] solution. Then, the solvent was removed by rotary evaporation at 50 °C for about 20 min. After that, the dried film was hydrated with filtered distilled water and the sample was sonicated for 5 min. Micelle dispersion was filtered through Phenex[®]-RC 0.22 μm filters (Phenomenex, Italy) to remove the unincorporated drug or possible large cylindrical aggregates formed by P123. When necessary, the resulting solution was freeze-dried for 24 h.

For Biotin-decorated PMM (Bio-PMM), biotin-conjugated F127 (20% of total F127 wt) was employed. For Rhodamine B-tagged PMM (Rho-PMM or Bio/Rho-PMM) rhodaminated-P123 (1% of total P123 wt) was used to give rhodamine B concentration of 5.0 μM. In the case of Bio/Rho-PMM micelles at 10 mg mL⁻¹, for example, 2.66 mg of F127 and 0.66 mg of biotin-conjugated F127, 6.60 mg of P123 and 0.066 mg of rhodamine B-conjugated P123 (a stock solution in ethanol of all the components) were used.

Recovery yield of the production process was evaluated on an aliquot of PMM dispersion by weighting the solid residue after freeze-drying. Results are expressed as the ratio of actual weight to the theoretical polymer weight × 100. Formulation optimization was assessed on the basis of micelle size, polydispersity index and NCL encapsulation efficiency.

2.4. Micelle characterization

Hydrodynamic diameter (D_H), polydispersity index (PI) and zeta potential of micelles were determined using a Zetasizer Nano ZS (Malvern Instruments Ltd., UK). The freeze-dried formulations were dispersed in Milli-Q water and measurements were performed at 37.0 °C on 90° angle. Results are reported as mean of three separated measurements on three different micelle batches (n = 9) ± standard deviation (SD). Bio/Rho-PMM morphology was evaluated by Transmission Electron Microscopy (TEM, JEOL JEM-1400, Jeol Ltd.-Japan) after negative staining with a 2% phosphotungstic acid solution.

The critical micelle concentration (CMC) of the Pluronic[®] mixture in aqueous PBS solutions was determined by fluorescence measurements using pyrene as fluorescent probe (Kalyanasundaram and Thomas, 1977). An aliquot (5 μL) of a pyrene stock solution in acetone (3.6 × 10⁻⁴ mol L⁻¹) was added into a series of test tubes, and the acetone was evaporated. Following this, micelle solutions at various concentrations (3.0 mL) were added to each test tube and sonicated for 2 h ([pyrene] = 6.0 × 10⁻⁷ mol L⁻¹). The excitation spectra were recorded (from 200 nm to 360 nm) with the emission wavelength fixed at 372 nm. The CMC was determined by I₃₃₇/I₃₃₄ intensity ratios from excitation spectra of pyrene.

The amount of biotin available on the surface of Bio-PMM was quantified by a competitive binding assay (HABA/avidin) (Bian et al., 2012). Rhodamine B-conjugated P123 was not included in the micelles to avoid interference in HABA/Avidin complex absorption. The powdered HABA/avidin reagent was reconstituted with 10 mL of deionized water. Thereafter, 900 μL of HABA/avidin solution were poured into a 1 mL cuvette. The absorption spectrum from 450 nm to 700 nm was collected and the absorbance at λ = 500 nm was recorded and indicated as A₅₀₀^{HABA/Avid}. Then, 100 μL of Bio-PMM were added into this solution. After extensive mixing, the

absorbance at λ = 500 nm was recorded and indicated as A₅₀₀^{HABA/Avid+sample}. The absorbance of the blank micelle solution at λ = 500 nm was indicated as A₅₀₀^{blanksample}.

The amount of the biotin actually exposed onto micelles was calculated by the following equation:

$$\frac{\mu\text{mol biotin}}{\text{mL}} = \left(\frac{34}{\Delta}\right) \times 10 \quad (1)$$

where $\Delta A_{500} = 0.9 \times A_{500}^{\text{HABA/Avid}} - A_{500}^{\text{HABA/Avid+sample}}$. The results are reported as mean of three separate measurements ± SD.

2.5. Niclosamide loading and release

NCL-loading was evaluated by measuring the UV-vis absorption after diluting the freshly prepared NCL-loaded PMM formulations in ethanol (1:100 v/v).

In vitro release of NCL from micelles was assessed by a dialysis method. A known amount of NCL-loaded micelles (40 mg) was dispersed in 1 mL of PBS or Dulbecco's Modified Eagle's Medium (DMEM) supplemented with 10% of fetal bovine serum (FBS) and placed in a dialysis bag (MWCO = 3500 Da, Spectra/Por[®]). The samples were plunged in 5 mL of 10 mM phosphate buffer at pH 7.4 containing 137 mM NaCl and 2.7 mM KCl (PBS) containing 0.5% v/v of polysorbate 80 in order to ensure sink conditions and to avoid NCL precipitation and kept at 37 °C. At selected time intervals, 1 mL of release medium was withdrawn, replaced with an equal volume of fresh medium and analysed. Release profile of free NCL (0.7 mg dissolved in 1 mL of ethanol or DMEM with 10% FBS medium) are reported for comparison. Results are expressed as mean release% over time (n = 3) ± SD.

The amount of NCL in the samples was measured at 331 nm on a Shimadzu 1800 spectrophotometer (Shimadzu, Italy) in a 1.0 cm quartz cuvette as previously reported (Costabile et al., 2015). Briefly, a calibration curve was obtained by plotting absorbance versus the concentration of NCL standard solutions in ethanol. The linearity of the response was verified over a concentration range of 0.2–10 μg/mL (r² = 0.998). The limit of detection and quantification were 0.24 μg/L and 0.80 μg/L, respectively. Unloaded micelles and release media had negligible absorption at 331 nm.

2.6. Cell cultures

Adenocarcinoma human alveolar basal epithelial (A549) and mouse embryo fibroblast (NIH3T3) cell lines were purchased from American Type Culture Collection (Rockville, MD, USA) and were authenticated by LGC Standards (Sesto San Giovanni, Italy). A549 and NIH3T3 cells were cultured in DMEM with glutamax (Invitrogen, Carlsbad, California) supplemented with 10% FBS, 2 mM L-glutamine and penicillin-streptomycin 50 U/ml.

2.7. Micelle uptake by fluorescence microscopy

A549 and NIH3T3 cells were plated on coverslips at a density of 2 × 10⁴ cells per well in 12-well plates. Then, cells were incubated with Rho-PMM and Bio/Rho-PMM (0.5 mg/mL) for 1, 4 and 24 h. Intracellular localization of micelles was monitored using a fluorescent microscope (Leica Microsystems GmbH, Wetzlar, Germany) to visualize 4',6-diamidino-2-phenylindole (DAPI) (345/661 nm) and Rhodamine-labelled micelles (557/571 nm). Fluorescence images were collected and processed by Axiovision 4.8.1 software. Images were processed, merged and reconstructed using Adobe Photoshop software. The scale bars on all the images correspond to 10 μm.

2.8. Cisplatin-resistant cell selection

A cisplatin-resistant A549 cell line (CPr-A549) was generated by continuously culturing the drug-sensitive parental cell line A549 in a medium containing increasing concentrations of cisplatin (from 0.5 μM to 14 μM) in a stepwise procedure over 10 months. After 10 months, the selected cells were 'pooled', in order to avoid clonality, and were tested to evaluate the rate of drug resistance, calculated as the resistance index, $\text{RI} = \text{IC}_{50} \text{CPr-A549} / \text{IC}_{50} \text{A549}$. Both cell lines were grown in DMEM medium containing 10% heat inactivated FBS, 50 U/ml penicillin, 500 $\mu\text{g/ml}$ streptomycin, 20 mM HEPES (pH 7.4) and 4 mM glutamine. The cells were grown in a humidified atmosphere composed of 95% air and 5% CO_2 at 37 °C.

2.9. Cell viability assays

For MTT assay, A549, CPr-A549 and NIH3T3 cells were seeded onto 96-well plates (2×10^4 cells/well) and incubated with micelles for 24 and 72 h. Then, cell viability was evaluated as mitochondrial activity using the MTT assay as previously reported (Maiolino et al., 2015). The absorbance was measured at 540 nm using a microplate reader (Labsystems Multiskan, MS).

For sulforhodamine B (SRB) colorimetric assay, cell viability of A549 and CPr-A549 cells was measured after 96 h of drug treatment in 96-well plates, as described previously (Milone et al., 2013).

2.10. Protein extraction and western blotting

Cells were grown and treated as indicated above, collected, lysed and separated on SDS polyacrylamide electrophoresis gels, and then proteins were transferred to nitrocellulose membranes (d'Emmanuele et al., 2015). Western blotting assay was performed as described previously (De Filippis et al., 2016) using antibodies anti-rpL3 (Primm, Milan, Italy), anti-p53, anti-p21, anti-LRP and anti-GAPDH (Santa Cruz Biotechnology, Santa Cruz, California), anti-ABCG2 (Cell Signaling), anti-MRP1 and anti-MDR1 (Abcam).

2.11. Clonogenic assay

For clonogenic assay, CPr-A549 cells were plated in triplicate at 4×10^3 in 6-well multidishes. At 10 days, colonies were stained with 1% methylene blue in 50% ethanol. Percent survival was normalized to the observed number of colonies generated from untreated cells.

2.12. Statistical analysis

Error bars represent mean \pm standard error mean (SEM) from $n=3$ biological replicates. Statistical comparisons were made by one-way ANOVA followed by Bonferroni's test for multiple comparisons. * #P < 0.05, ** ## P < 0.01, *** P < 0.005. P > 0.05 was considered not statistically significant.

3. Results

3.1. Pluronic[®] functionalized with biotin or rhodamine B: synthesis, assembling properties and cell uptake

Multifunctional micelles were prepared from F127 and P123 reacted at hydroxyl end groups with biotin as targeting agent or rhodamine B as fluorescent tag, respectively. ^1H NMR spectra of modified polymers (Fig. 1A and B) showed the main peaks corresponding to the PPO (1.0–1.2 ppm) and PEO (3.2–3.6 ppm) segments. Most of biotin signals were overlapped to polymers signals (Fig. 1A) although the multiple signals at 4.138 ppm (H_6),

4.300 ppm (H_6) and the singlet signals at 6.363 ppm ($\text{H}_{\text{N}2}$) and 6.437 ppm ($\text{H}_{\text{N}1}$) confirmed biotin-F127 conjugation. For the rhodamine-conjugated P123 (Fig. 1B), the aromatic signals above 7 ppm confirm Rhodamine conjugation to P123 molecules.

Suggestion that modified polymers could self-assemble with unmodified ones to form mixed micelles was given by comparing ^1H NMR in DMSO- d_6 and D_2O as solvents. In fact, DMSO- d_6 is a good solvent for all components and signals referring to all the species could be detected (Fig. 1A and B). Nevertheless, D_2O is a good solvent for biotin, rhodamine B and PEO blocks while lipophilic PPO blocks are poorly soluble in water, driving the formation of the micelle core. In fact, NMR signals originating from hydrophobic PPO blocks were suppressed in water due to PPO restricted motion in the micelle core (Fig. 1C).

Bio-PMM were prepared at 2:1 (w/w) P123 and F127 ratio on the basis of our previous study (Pellosi et al., 2016). The CMC of P123/F127 mixture in the presence of Biotin-conjugated F127 was 0.0031% w/V, as evaluated by pyrene method (Fig. 2A). Analogously, addition of Rho-conjugated P123 did not alter Bio-PMM properties (data not shown). The availability of biotin on micelle surface was also quantified by measuring the absorbance of the HABA/avidin complex at 500 nm (Fig. 2B) (Bian et al., 2012). The theoretical amount of available biotin on Bio-PMM was 1.25 $\mu\text{mol mL}^{-1}$, corresponding to 10% of biotin at a micelle concentration of 10 mg mL^{-1} . The actual available amount of biotin was 1.04 $\mu\text{mol mL}^{-1}$, which means that approximately 8.3% of the micelle surface is covered with biotin. Bio-PMM were almost spherical as shown in the TEM image reported in Fig. 2C.

The uptake and the subcellular distribution of unloaded Rho-PMM and Bio/Rho-PMM were assessed in biotin receptor-positive A549 cells and in a non-cancerous cell line NIH3T3 as control. After a time-dependent incubation with micelles (1, 4 and 24 h), the cells were stained with DAPI and observed by fluorescence microscopy. In A549 cells, the large majority of the fluorescence associated to Bio/Rho-PMM was distributed in the cytoplasm, confirming micelle internalization (Fig. 3). The quantification of fluorescence revealed a time-dependent uptake of the micelles. In normal NIH3T3 fibroblasts, a very limited internalization of both Rho-PMM and Bio/Rho-PMM was found (Fig. 4).

3.2. NCL-loaded PMM: properties and cytotoxicity in A549 cells

Table 1 summarizes the physicochemical characteristics and drug-loading parameters of NCL-loaded PMM. In each case, PMM with increased PI and a hydrodynamic diameter within the range 25–35 nm were achieved as compared to unloaded PMM (Table 1). Zeta potential values were slightly negative independently of the drug amount loaded (Table 1) as generally found for uncharged PEO-coated nanocarriers due the high electronic density of oxygen (Conte et al., 2014). Of note, both micelle size and charge were not affected by the presence of the small and neutral biotin molecule on micelle surface at present conditions. The encapsulation efficiency strongly depended upon Pluronic[®]/NCL ratio by weight. High ratios resulted in good encapsulation efficiencies while the opposite effect was observed at lower Pluronic[®]/NCL ratios, likely due to drug precipitation during preparation. The optimal formulation condition for NCL encapsulation was at 40 mg mL^{-1} for Pluronic[®] mixture and 0.7 mg mL^{-1} for NCL. Blank micelles at same polymer concentration (control experiment) presented a size of 29.5 nm (PI = 0.142) and zeta potential of -3.81 mV.

Release profile of NCL from NCL-loaded Bio-PMM in PBS at pH 7.4 was evaluated by dialysis method (Fig. 5). NCL displayed a biphasic release profile with an initial burst (first 6 h) followed by a sustained release phase lasting up to 48 h. The drug could freely diffuse through the dialysis membrane as demonstrated in control experiments. Release profile in the DMEM supplemented with 10%

of FBS followed a biphasic pattern again, which occurred at a rate slower than in PBS (Fig. 5).

In the light of the promising technological features, we tested the cytotoxicity of the optimized NCL-loaded micelles in A549

cancer cells and normal NIH3T3 fibroblasts. To this aim, cytotoxicity of NCL-loaded micelles incubated in a wide range of concentrations ($1.3\text{--}112\ \mu\text{g mL}^{-1}$ corresponding to $0.07\text{--}6\ \mu\text{M}$ of

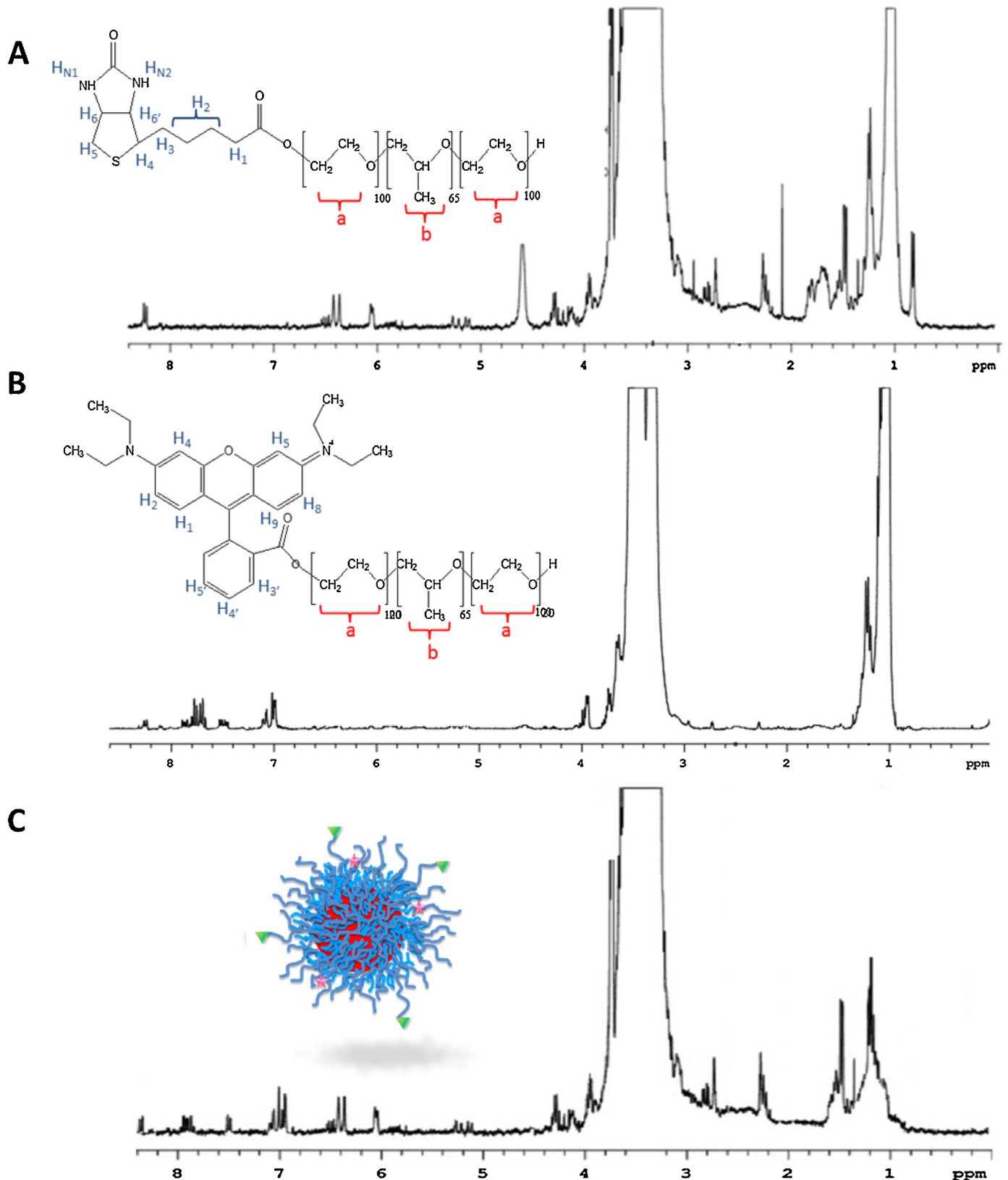


Fig. 1. ^1H NMR spectra of: (A) biotin-conjugated F127 in $\text{DMSO-}d_6$; (B) rhodamine B-conjugated P123 in $\text{DMSO-}d_6$; (C) Bio/Rho-PMM in D_2O .

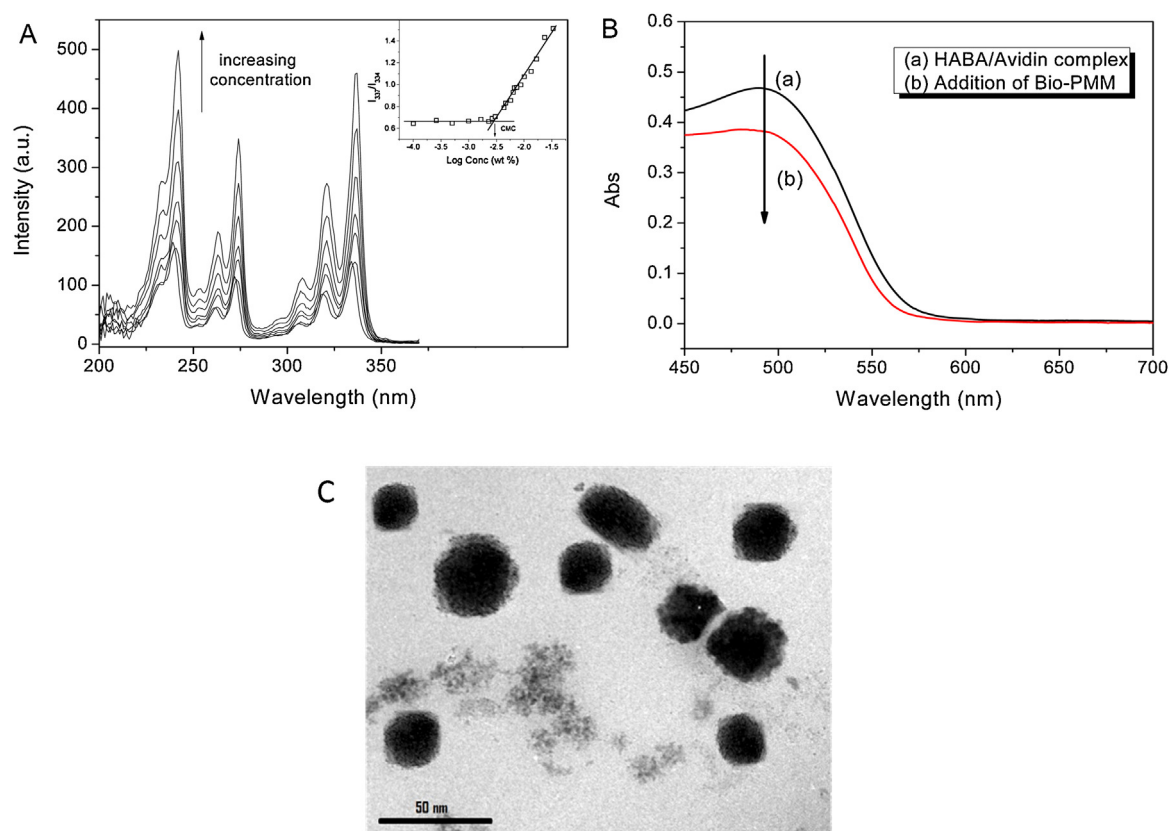


Fig. 2. Properties of Bio-PMM. (A) Fluorescence excitation spectra of pyrene ($6.0 \times 10^{-7} \text{ mol L}^{-1}$) as a function of the concentration of Bio-PMM in PBS at pH 7.4 and 37 °C. The inset shows the plot of the intensity ratio (I_{337}/I_{334}) from the fluorescence excitation spectra of pyrene at 372 nm as a function of logarithm concentration of PMM. (B) UV-vis spectra of the HABA/Avidin complex and HABA/Avidin complex after Bio-PMM addition. (C) TEM image of Bio/Rho-PMM.

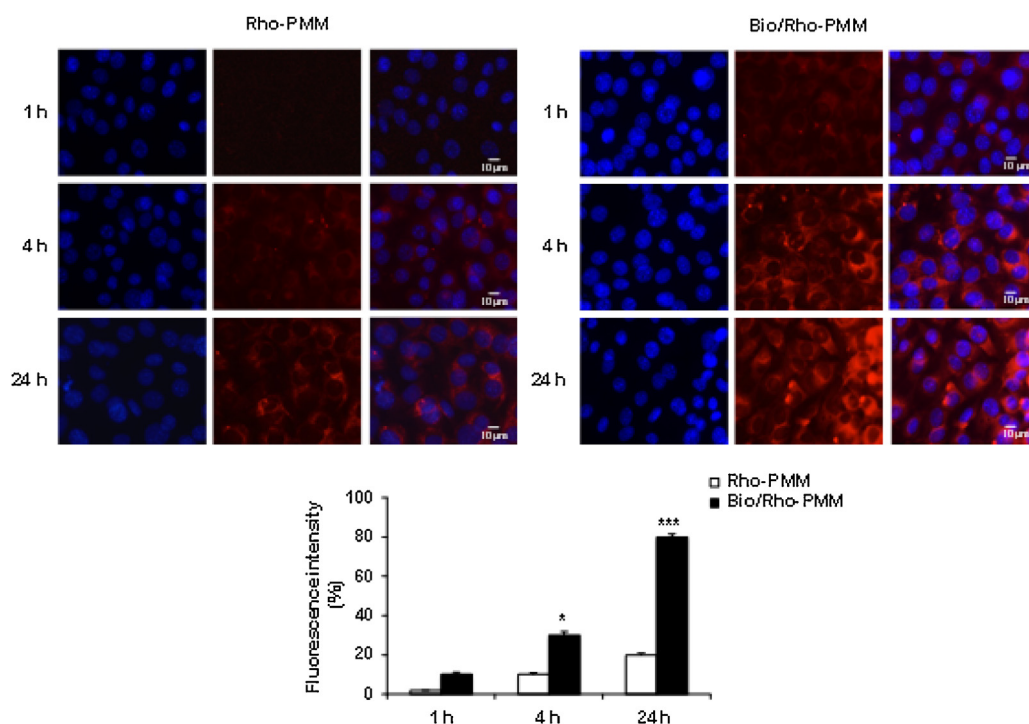


Fig. 3. Fluorescence microscopy images of A549 cells after incubation with Rho-tagged micelles. A549 cells were incubated with Rho-PMM and Bio/Rho-PMM (0.5 mg/mL) for 1, 4 and 24 h. Cell nuclei were stained with DAPI. Fluorescence images were collected and processed by Axiovision 4.8.1 software. All measurements were normalized to the fluorescence of Bio/Rho-PMM in cell medium set as 100%. Bars represent mean values \pm SEM of experiments done in triplicate. * $P < 0.05$, *** $P < 0.005$.

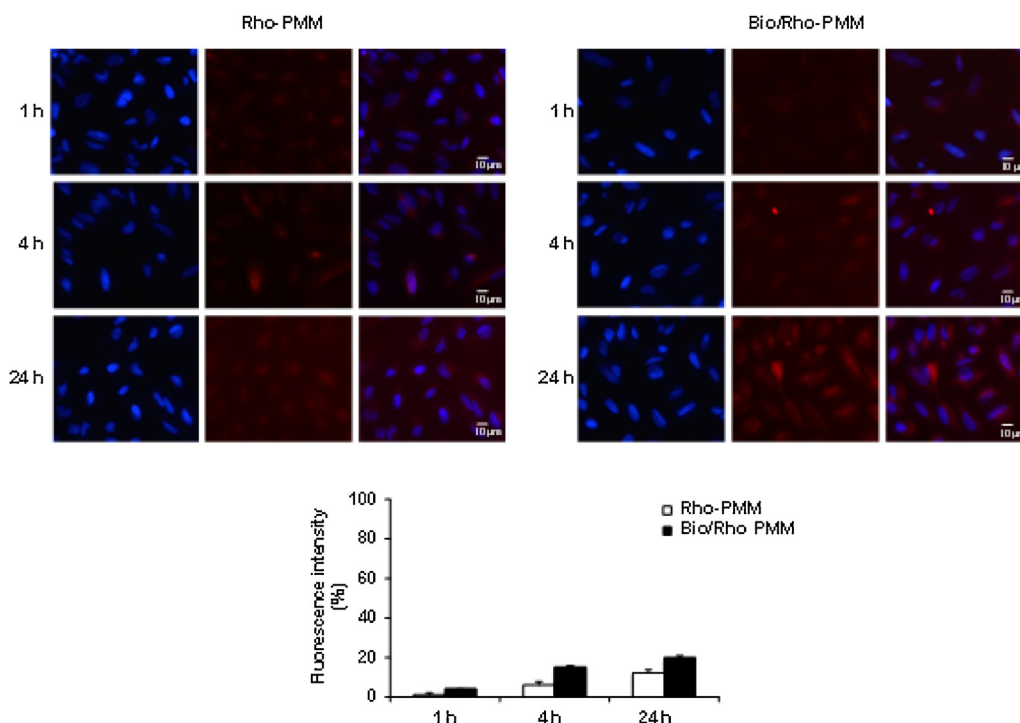


Fig. 4. Fluorescence microscopy images of NIH3T3 cells after incubation with Rho-tagged micelles. NIH3T3 cells were incubated with Rho-PMM and Bio/Rho-PMM (0.5 mg/mL) for 1, 4 and 24 h. Cell nuclei were stained with DAPI. Fluorescence images were collected and processed by Axiovision 4.8.1 software. All measurements were normalized to the fluorescence of Bio/Rho-PMM in cell medium set as 100%. Bars represent mean values \pm SEM of experiments done in triplicate.

Table 1

Composition and properties of NCL-loaded Bio-PMM. Results reported as average of three separated measurements on three different batches (n=9) \pm SD.

Pluronic [®] (mg mL ⁻¹) ^a	NCL (mg mL ⁻¹)	ratio Plur/NCL	Yield (%)	NCL actual loading \pm SD ^b (EE \pm SD) ^c	Mean D _H (nm \pm SD)	P.I.	Zeta potential (mV \pm SD)
10	0.1	100	95	0.913 \pm 0.043 (91.5 \pm 1.2)	27.4 \pm 1.8	0.132	-3.91 \pm 0.67
10	0.2	50	89	1.33 \pm 0.10 (67.8 \pm 1.8)	35.9 \pm 2.4	0.266	-4.59 \pm 1.15
10	0.3	33	89	1.72 \pm 0.26 (59.0 \pm 3.1)	28.2 \pm 4.7	0.345	-3.33 \pm 1.89
20	0.1	200	92	0.495 \pm 0.014 (99.2 \pm 1.2)	25.2 \pm 1.2	0.138	-4.01 \pm 0.88
20	0.3	67	85	1.24 \pm 0.052 (88.4 \pm 3.4)	24.2 \pm 2.3	0.178	-3.89 \pm 1.01
20	0.5	40	91	1.62 \pm 0.073 (66.4 \pm 4.1)	20.2 \pm 3.7	0.351	-5.49 \pm 2.48
30	0.5	60	90	1.54 \pm 0.38 (93.9 \pm 2.0)	28.4 \pm 2.5	0.152	-4.62 \pm 1.61
40	0.7	57	94	1.58 \pm 0.55 (91.9 \pm 1.9)	31.8 \pm 1.7	0.131	-3.37 \pm 1.08
50	0.7	71	88	1.29 \pm 0.27 (93.4 \pm 4.1)	26.5 \pm 2.5	0.129	-5.49 \pm 2.07
50	1.0	50	93	1.81 \pm 0.49 (92.3 \pm 4.1)	33.4 \pm 3.9	0.246	-2.21 \pm 0.88

^a P123/F127 mixture 2:1 w/w where biotin-conjugated F127 was used at 20% of F127 mass.

^b Actual loading is expressed as the amount (mg) of drug encapsulated per 100 mg of Bio-PMM \pm SD.

^c Entrapment efficiency (EE) is expressed as the ratio between experimental and theoretical NCL loading \times 100 \pm SD.

NCL) was evaluated after 72 h exposure by using MTT assay and compared to that of free NCL (Fig. 6).

Results indicated that NCL-loaded Bio-PMM micelles were significantly more cytotoxic than NCL and NCL-loaded PMM in A549 cells (Fig. 6A). No significant difference in cytotoxicity between free NCL and NCL-loaded micelles was found in NIH3T3. Unloaded PMM and Bio-PMM did not show any cytotoxicity toward both cell lines at any concentration tested (Fig. S1, Supplementary material). Data from MTT at 24 h highlight that cytotoxicity was

again significantly higher for NCL-loaded Bio-PMM (Fig. S2, Supplementary material).

3.3. In vitro activity of NCL-loaded PMM against resistant lung cancer cells

A cisplatin-resistant subline derived from the parental sensitive cell line A549 was successfully established. A549 cells were continuously selected with cisplatin over a period of 10 months in

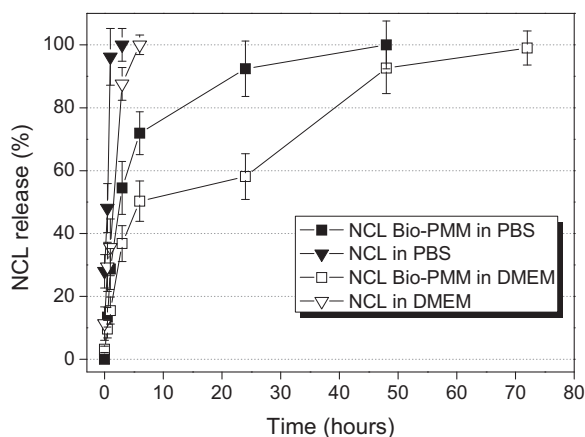


Fig. 5. Release profiles of NCL and NCL-loaded Bio-PMM dispersed in PBS and in DMEM supplemented with FBS 10%. Free NCL is reported as control. The external medium used for dialysis was PBS with polysorbate 80 (0.5% v/v) at pH 7.4 and at 37 °C. NCL concentration in the bag was 0.7 mg mL⁻¹. Data are reported as mean of three independent experiments (n = 3) ± SD.

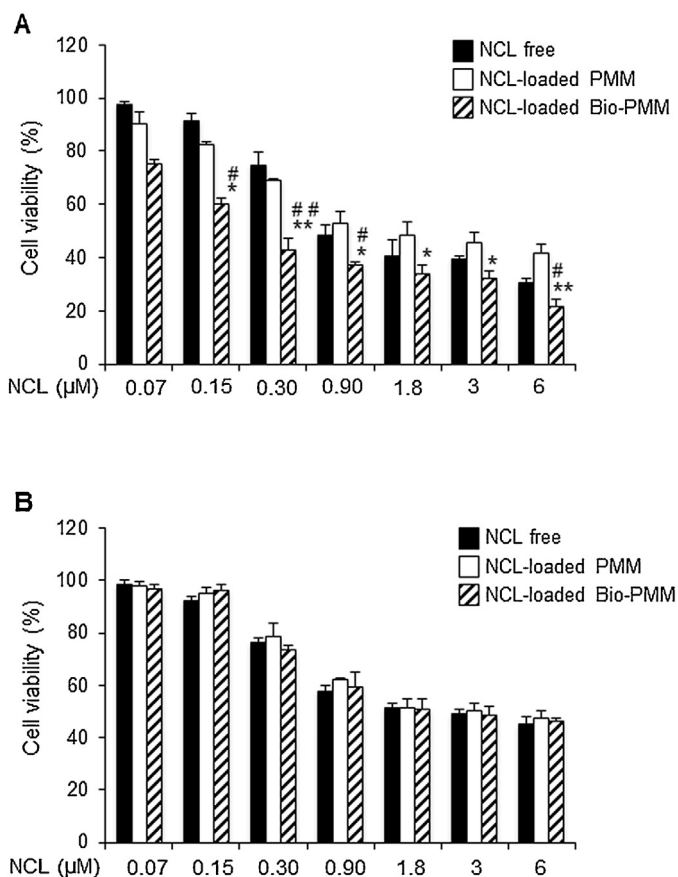


Fig. 6. *In vitro* cytotoxicity of free NCL and NCL-loaded micelles toward A549 (A) and NIH3T3 (B) cells. The cells were exposed to increasing concentrations of PMM (1.3–112 μg mL⁻¹ corresponding to 0.07–6 μM of NCL) or NCL in DMSO (0.07–6 μM) for 72 h. After incubation, cell viability was evaluated using the MTT assay. The cell viability from untreated cells was set to 100%. Results are presented as percentage (mean ± SEM) (n = 3) of the control cells. *, ** NCL-loaded Bio-PMM vs NCL-loaded PMM. ### NCL-loaded Bio-PMM vs NCL. * #P < 0.05, ** ##P < 0.01.

order to generate corresponding age and passage-matched cisplatin-resistant cell line, designated as CPr-A549. Maintenance of the resistant subline was continued at 14 μM. The SRB

proliferation assay demonstrated an increased resistance to cisplatin-induced cell death (Fig. 7A). Specifically, the drug-adapted CPr-A549 cell line showed a significantly higher IC₅₀ compared with parental A549 cells (13.3 ± 4 versus 3.8 ± 0.4, respectively; P < 0.05), resulting in more than 3-fold resistance to cisplatin (Table 2). In addition, we demonstrated a significant increase in the IC₅₀ of CPr-A549 cells compared to A549 cells (Table 2) to other conventional chemotherapeutic drugs such as docetaxel (Fig. 7B), 5'-deoxy-5-fluorouridine (5'-DFUR) (Fig. 7C) and 5-fluorouracil (5-FU) (Fig. 7D). These results indicate that CPr-A549 cells show resistance to multiple drugs representing an interesting tool to study MDR in lung cancer.

The effect of free NCL on CPr-A549 cell line viability was first investigated. To this purpose, cells were exposed to a wide range of NCL concentrations (ranging from 0.07 to 6 μM) and *in vitro* cytotoxicity evaluated by using MTT assay. Fig. 8A shows the dose-response effect after 72 h of treatment with free NCL giving an IC₅₀ value of 1.8 μM. This result demonstrated that NCL can overcome resistance to different chemotherapeutics in CPr-A549 cells.

To go in depth into molecular mechanism underlying MDR in CPr-A549 cells, the expression profile of ATP binding cassette (ABC) efflux pumps ABCG2, lipoprotein receptor-related protein (LRP) was evaluated. The expression level of multi-drug resistance 1/P-glycoprotein (MDR1) and MDR-associated protein 1 (MRP1) was also analyzed. Western blotting analysis showed no difference in the expression of such proteins in CPr-A549 cells as compared with the parental A549 cells (Fig. 8B).

To investigate whether NCL cytotoxic effect on CPr-A549 cells was associated to nucleolar stress, protein extracts from CPr-A549 cells treated or not with free NCL were analyzed by western blotting for the expression profile of rPL3 and its target p21 protein. We found that the resistance of A549 cells to cisplatin correlated to the loss of rPL3 expression (Fig. 8C). NCL treatment caused a significant increase of rPL3 level that was associated to the up-regulation of p21.

The antiproliferative activity of NCL-loaded micelles towards multidrug-resistant CPr-A549 cancer cells was finally investigated (Fig. 9). After 3 days of treatment, *in vitro* cytotoxicity was first evaluated by MTT assay. Extrapolation from the dose-response curve demonstrated that cytotoxicity of NCL-loaded Bio-PMM was higher than that of NCL-loaded PMM (and free NCL) depending on the dose (Fig. 9A). To exclude definitively that treated cells retained any capacity to divide and to proliferate, the *in vitro* effectiveness of NCL-loaded Bio-PMM against CPr-A549 cells was also assessed through a clonogenic assay. The assay was performed after treatment of CPr-A549 cells with 0.3, 0.9 and 1.8 μM of NCL-loaded Bio-PMM for 72 h. As can be seen in Fig. 9B, after 10 days the colony number was strongly reduced upon exposure to drug-loaded Bio-PMM confirming the ability of NCL to inhibit clonogenicity.

4. Discussion

An increasing resistance of cancer cells to the treatment with commonly used chemotherapeutic drugs has raised the urgency in the search for new anti-cancer agents. Several drugs originally approved for indications other than cancer therapy have recently been found to exert a cytotoxic effect on cancer cells (Shim and Liu, 2014; Stenvang et al., 2013). Cisplatin represents the first line chemotherapy for the treatment of a variety of tumors, including non-small cells lung cancer (NSCLC), and platinum resistance is a major limitation in the treatment of NSCLC. Recent studies focusing on the anthelmintic drug NCL demonstrate its ability to overcome drug resistance in different cancers (Li et al., 2013; Liu et al., 2015, 2014).

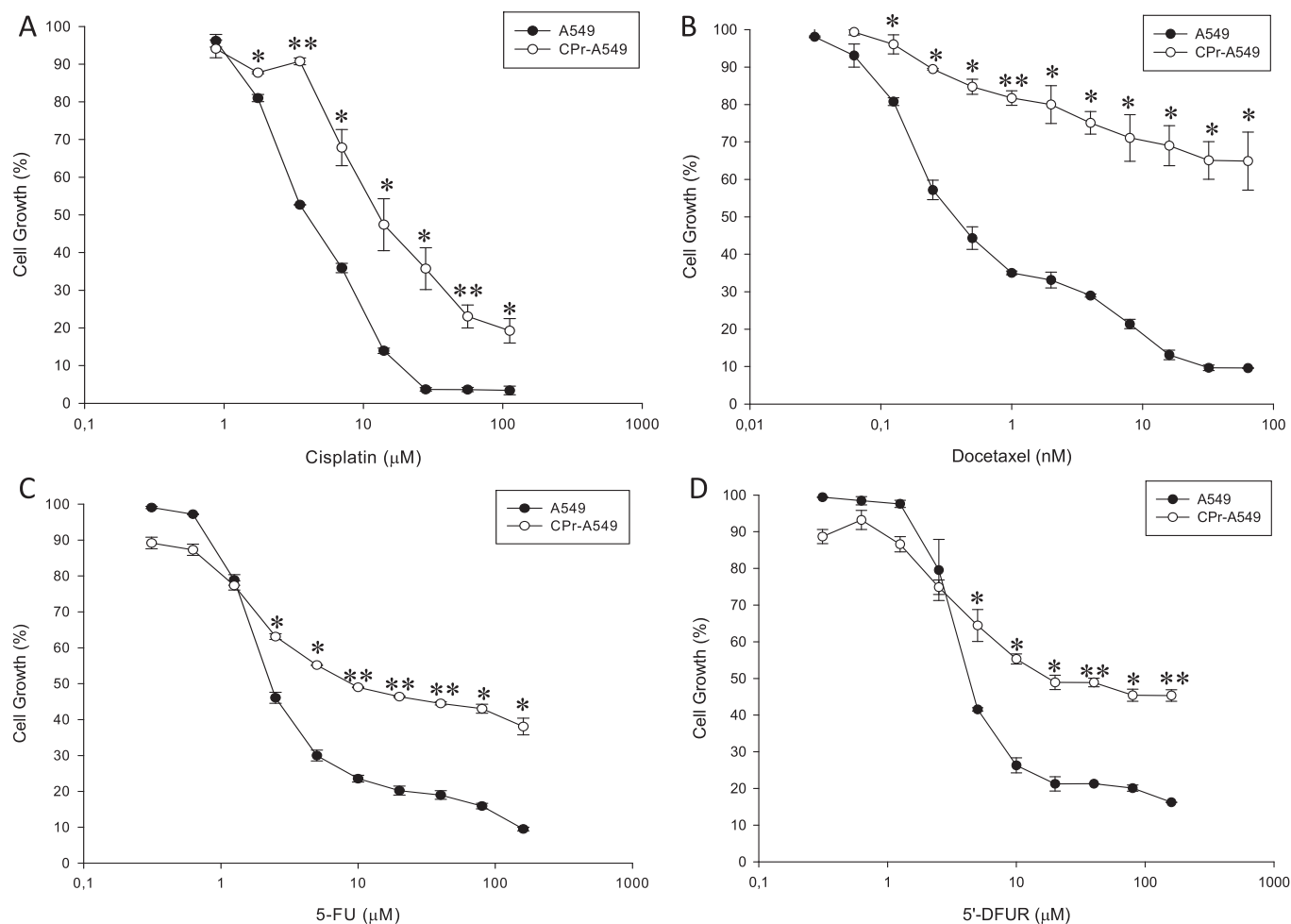


Fig. 7. Development of cisplatin-resistant NSCLC cell line. Sensitive A549 cells and CPr-A549 cells were treated with increasing concentrations of (A) Cisplatin, (B) Docetaxel, (C) 5-FU or (D) 5'-DFUR for 96 h and cell growth assessed by SRB colorimetric assay. Cell growth is expressed as percentage of control for each time point. Values are the mean \pm SD from at least three independent experiments performed in quadruplicates. * $P < 0.05$, ** $P < 0.01$.

Table 2

Antiproliferative effect of anticancer drugs on sensitive A549 and cisplatin-resistant A549 cells (CPr-A549). Resistance index (RI) is reported as IC_{50} CPr-A549/ IC_{50} A549.

	IC_{50} (μ M)	
	A549	CPr-A549
Cisplatin	3.8 ± 0.4	13.3 ± 4 (RI = 3.5)
Docetaxel	$0.54 \times 10^{-3} \pm 0.05 \times 10^{-3}$	$> 64 \times 10^{-3}$ (RI > 164)
5-FU	2.55 ± 0.07	8.9 ± 0.28 (RI = 3.45)
5'-DFUR	4.65 ± 0.35	17.98 ± 3.7 (RI = 3.97)

Despite promising, the translation of NCL-based chemotherapy *in vivo* runs into special difficulties, mainly related to the very poor solubility profile of NCL in biological fluids. To overcome NCL solubility constraints, Pluronic[®] P123/F127 mixed micelles (PMM) for targeted delivery of NCL to lung cancer cells were built up.

In a previous work, we demonstrated that PMM made of 2:1 (w/w) mixtures of P123 and F127 display high stability to dilution and can load highly hydrophobic benzoporphyrin derivatives (Pellosi et al., 2016). Here, PMM were surface-engineered to encourage cell internalization by exposing biotin on their surface. PMM were also made fluorescent by linking Rhodamine B to micelle surface to track their trafficking inside cells. Biotin and rhodamine B were linked to Pluronic[®] unimers at their hydroxyl-termination using carbodiimide chemistry (Li et al., 2010). We decided to conjugate

biotin to F127, bearing longer PEO blocks, while rhodamine B was linked to P123, with shorter PEO chains. Through this design, it was expected that targeting ligand exposition on micelle surface is attained and any interference between biotin and rhodamine is minimized, which is a key prerequisite for micelle-receptor recognition. NMR analyses provided insight into the occurrence of the self-assembly of the two Pluronic derivatives, indicating the formation of a well-defined core-shell structure in aqueous solution where a "water-protected" PPO core is surrounded by a PEO hydrophilic coating exposing biotin as targeting element and rhodamine B as fluorescent tag. Indeed, complex formation of Bio-PMM with avidin clearly indicates that biotin was surface-exposed and potentially able to interact with receptors on cell membranes (Bian et al., 2012). Meanwhile, the reasonably low CMC value indicated a good stability of targeted PMM to dilution being promising for their potential applications as drug carrier.

Aiming at demonstrating the soundness of this approach to promote NCL accumulation in cancer cells, the uptake and the subcellular distribution of unloaded Rho-PMM and Bio/Rho-PMM were assessed in biotin receptor-positive lung A549 cancer cells and in a non-cancerous NIH3T3 cell line. Results demonstrated a higher amount of biotin-decorated PMM in cancer cells as compared to normal cells. Thus, the overexpression of biotin receptors on the surface of A549 cancer cells relative to normal NIH3T3 cells, induced a higher micelle uptake by receptor-

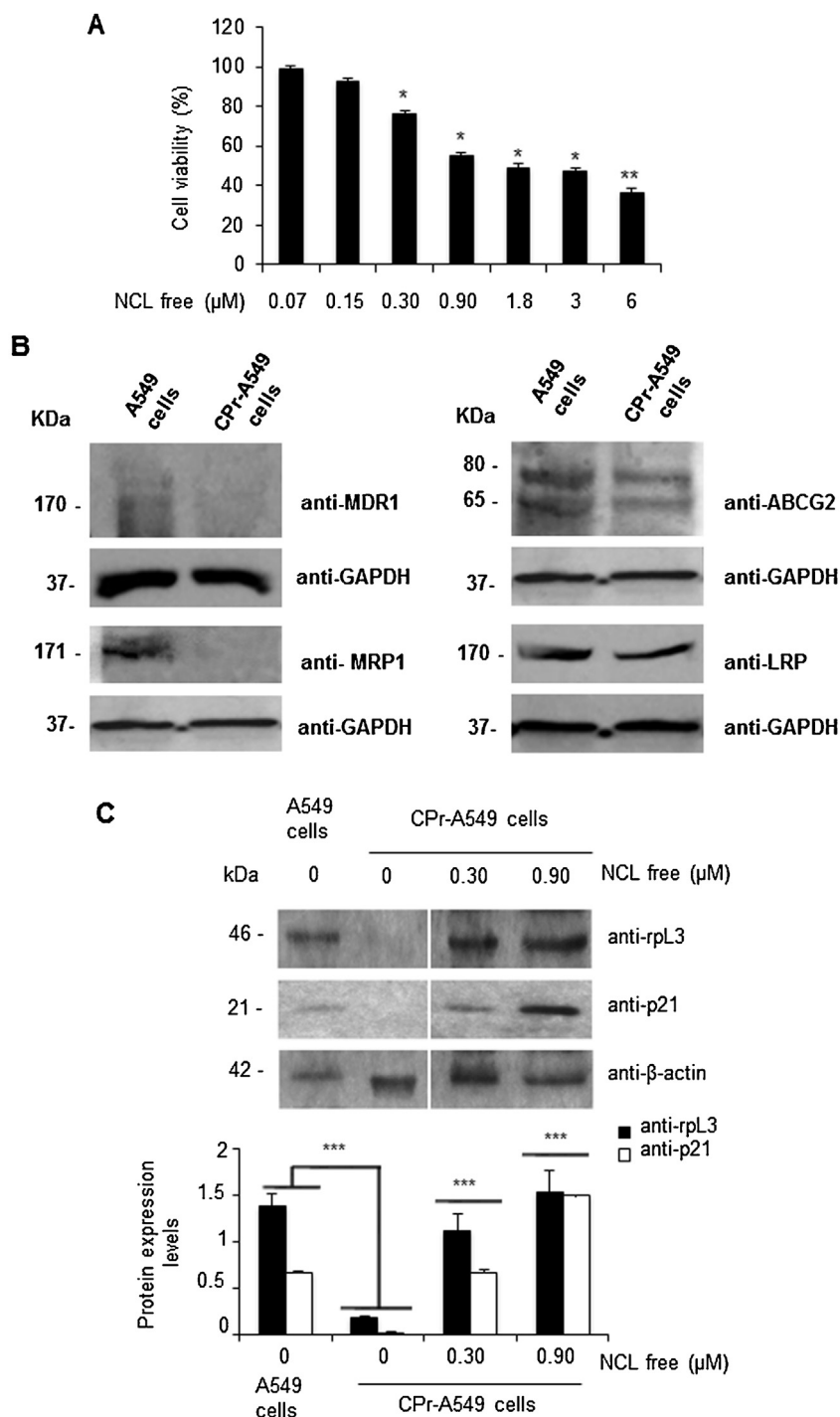


Fig. 8. Effect of NCL in CPr-A549 cells. (A) *In vitro* cytotoxicity of NCL (0.07–6 μM) toward CPr-A549 cells after 72 h. Cell viability was evaluated by MTT assay. The cell viability from untreated cells was set to 100%. Results are presented as percentage (mean ± SEM) ($n = 3$) of the control cells. * $P < 0.05$, ** $P < 0.01$. (B) Expression profile of MDR1, ABCG2, MRP1 and LRP, in CPr-A549 cells. Protein extracts from A549 cells (control) and CPr-A549 cells were analysed by western blotting by using anti-MDR1, anti-ABCG2, anti-MRP1, anti-LRP and anti-GAPDH to normalize. (C) Analysis of rpL3 and p21 expression upon NCL treatment in CPr-A549 cells. Protein extracts from A549 cells (control) and CPr-A549 cells, untreated or treated with free NCL, were analysed by western blotting by using anti-rpL3, anti-p21 and anti-β-actin to normalize results. Quantification of signals is shown. Bars represent mean values ± SEM of experiments done in triplicate. *** $P < 0.005$.

mediated endocytosis (Heo et al., 2012; Jung et al., 2014; Maiti et al., 2013).

The feasibility of the proposed approach for selective delivery of NCL in lung cancer cells was then assessed. To this purpose, preliminary studies were devoted to the development of Bio-PMMA, affording high encapsulation efficiency of NCL at the minimum Pluronic®/NCL ratio (i.e. higher drug loading for micelle). The key

factor for formulation optimization was the dependence of the encapsulation efficiency on Pluronic/NCL weight ratio. Values between 50 and 60 were considered suitable for a therapeutically-relevant system. Besides a slight size increase after entrapment of the drug, likely ascribable to drug entangling in the PPO core, the micelles were still small enough for tumor-specific accumulation via the EPR effect (Batrakova and Kabanov, 2008). Furthermore, the

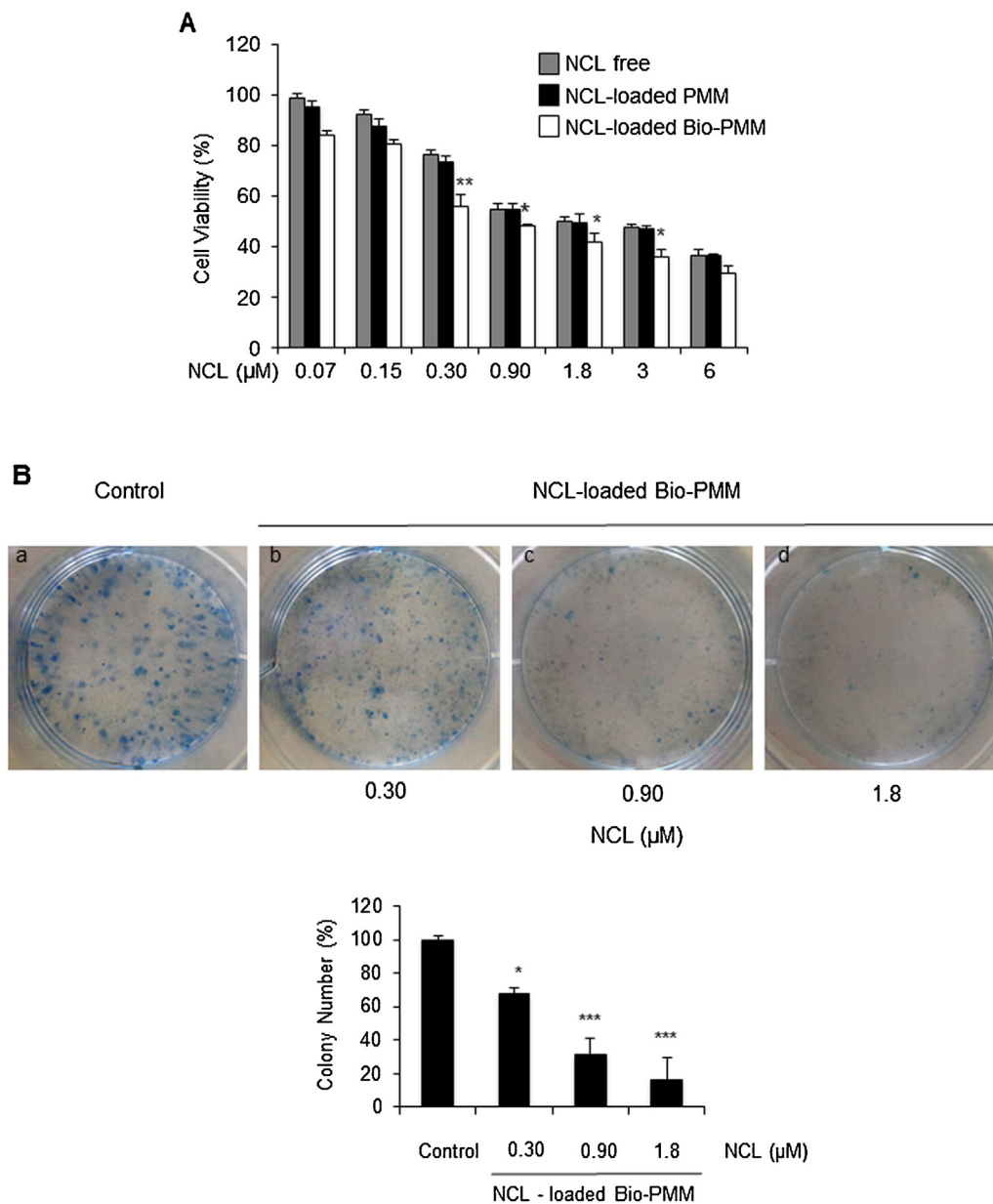


Fig. 9. *In vitro* cytotoxicity of NCL-loaded micelles in CPr-A549 cells. (A) CPr-A549 cells were exposed to increasing concentrations of micelles (1.3–112 $\mu\text{g mL}^{-1}$ corresponding to 0.07–6 μM of NCL) for 72 h. After incubation, cell viability was evaluated by MTT assay. Cytotoxicity of NCL from Fig. 8 is reported to facilitate comparison. The cell viability from untreated cells was set to 100%. Results are presented as percentage (mean \pm SEM) ($n = 3$) of the control cells. * $P < 0.05$, *** $P < 0.005$. (B) Clonogenic assay on CPr-A549 cells treated with 0.3, 0.9 and 1.8 μM of NCL for 72 h or untreated. After 10 days, colonies were stained with methylene blue, counted and photographed. Bar chart indicating clonogenic growth is shown. * $P < 0.05$, ** $P < 0.01$, *** $P < 0.005$.

developed delivery platform allowed for a slow release of NCL, also in a complex protein-rich milieu, such as the cell culture medium employed for *in vitro* experiments.

Prompted by these encouraging findings, the *in vitro* anti-proliferative effect of the selected NCL-loaded Bio-PMM was investigated in lung cancer cells, as well as in normal cells. NCL-loaded Bio-PMM displayed an enhanced cytotoxic activity in A549 cells as compared to healthy cells, which correlated well with their higher intracytoplasmic accumulation.

For a better understanding of the therapeutic potential of NCL-loaded Bio-PMM and to investigate the molecular basis of NCL cytotoxic activity, we successfully established a cisplatin-resistant lung cancer subline derived from the parental sensitive cell line A549 (CPr-A549 cells), which demonstrated resistance also to other conventional chemotherapeutics. Drug resistance may be

due to decreased influx or increased efflux of drugs (Rabik and Dolan, 2007). Several ABC transporter efflux inhibitors have been described (Schinkel and Jonker, 2003) and it is well established that the transmembrane ATP binding cassette (ABC) efflux pumps ABCB1 (P-glycoprotein, P-gp), ABCC1 (MDR-associated protein 1, MRP1), and ABCG2 (breast cancer resistance protein, BCRP) play a crucial role in the development of drug resistance (Eckford and Sharom, 2009). Our results clearly indicate that the development of MDR in CPr-A549 cells was not the result of the overexpression of neither ABCG2 and LRP, nor MDR1 and MRP1 suggesting the involvement of other pathways.

Recently our studies focused on the extraribosomal functions of ribosomal proteins (Russo et al., 2011, 2010), with particular attention to their role in chemotherapy and chemoresistance (Pagliara et al., 2016). Specifically, we demonstrated that

ribosome-free rpl3 plays a crucial role in cell response to nucleolar stress induced by anticancer drugs such as 5-Fluorouracil (5-FU), Actinomycin D and oxaliplatin (Esposito et al., 2014; Russo et al., 2016). In fact, upon drug-induced nucleolar stress, free rpl3 is able to induce cell cycle arrest, apoptosis and to inhibit cell proliferation and migration by controlling p21 expression both at post-transcriptional and post-translational levels. Furthermore, we demonstrated that rpl3 status was associated to chemoresistance since the loss of rpl3 makes the tested chemotherapeutic drugs ineffective (Esposito et al., 2014; Russo et al., 2016). In agreement with our previous results, CPr-A549 cells resistance to cisplatin correlated to the loss of rpl3 expression. It is noteworthy that NCL caused a significant increase of rpl3 level that was associated to the up-regulation of p21. These data reveal that a novel molecular mechanism implicated in the cytotoxic activity of NCL can be hypothesized, involving nucleolar stress and rpl3/p21 response pathway.

Of note, results on CPr-A549 cells demonstrated not only that NCL is still active in resistant lung cancer cells but also that biotin-targeted PMM maintain their cytotoxicity profile being more cytotoxic than non-targeted micelles, especially at low concentrations. These results point at biotin-decorated PMM as a reasonable strategy to improve NCL activity also in resistant lung cancer cells, which, after treatment, become definitively unable to divide and to proliferate.

5. Conclusions

With this study we demonstrate that NCL delivered through tailored Pluronic[®] mixed micelles can be a valuable therapeutic tool in the treatment of multi-drug resistant NSCLC. Biotin-targeted Pluronic mixed micelles designed for intravenous injection entrapped NCL with good yield, showed sustained NCL release and were stable in protein-rich media. As compared to normal NIH3T3 fibroblasts, biotin-targeted micelles were internalized much more efficiently and exerted a more potent cytotoxicity than that of both free NCL and non-targeted micelles in A549 cells. After selecting a resistant A549 cell line, we identified rpl3 and p21 as new molecular targets of NCL and demonstrated that the activation of rpl3/p21 pathway by NCL overcomes MDR. Superior cytotoxicity of NCL-loaded biotin-targeted micelles was clearly evidenced in A549 cell resistant to cisplatin, 5-FU and docetaxel while the clonogenic assay demonstrated that, after treatment, cells becomes unable to divide and to proliferate. Taken all together, these results demonstrate that a NCL-based regimen with biotin-decorated Pluronic micelles might be a promising second-line chemotherapy for lung cancer showing cisplatin or multi-drug resistance.

Conflicts of interest

All authors declare no conflicts of interest.

Acknowledgments

F.Q. and G.R. wish to thank the Italian Ministry of University and Research (PRIN 2010H834LS, PRIN20104AE23N_006). F.Q. wishes also to thank Italian Association for Cancer Research (IG2014, #15764) for financial support. F.U. gratefully acknowledges *Compagnia di San Paolo* and *Istituto Banco di Napoli—Fondazione (STAR Program, Junior Principal Investigator Grant 2013, Napoli-call2013_35)* for financial support.

D.S.P and N.H. wishes to thank the Brazilian agency Coordenação de Aperfeiçoamento de Pessoal de Nível Superior (CAPES) process number BEX 14036/13-14.

Appendix A. Supplementary data

Supplementary data associated with this article can be found, in the online version, at <http://dx.doi.org/10.1016/j.ijpharm.2016.06.118>.

References

- Alakhova, D.Y., Kabanov, A.V., 2014. Pluronics and MDR reversal: an update. *Mol. Pharm.* 11, 2566–2578.
- Alvarez-Lorenzo, C., Sosnik, A., Concheiro, A., 2011. PEO-PPO block copolymers for passive micellar targeting and overcoming multidrug resistance in cancer therapy. *Curr. Drug Targets* 12, 1112–1130.
- Ashburn, T.T., Thor, K.B., 2004. Drug repositioning: identifying and developing new uses for existing drugs. *Nat. Rev. Drug Discov.* 3, 673–683.
- Balgi, A.D., Fonseca, B.D., Donohue, E., Tsang, T.C., Lajoie, P., Proud, C.G., Nabi, I.R., Roberge, M., 2009. Screen for chemical modulators of autophagy reveals novel therapeutic inhibitors of mTORC1 signaling. *PLoS One* 4, e7124.
- Batrakova, E.V., Kabanov, A.V., 2008. Pluronic block copolymers: evolution of drug delivery concept from inert nanocarriers to biological response modifiers. *J. Control Release* 130, 98–106.
- Bian, Q., Xiao, Y., Lang, M., 2012. Thermoresponsive biotinylated star amphiphilic block copolymer: synthesis self-assembly, and specific target recognition. *Polymer* 53, 1684–1693.
- Chen, S., Zhao, X., Chen, J., Chen, J., Kuznetsova, L., Wong, S.S., Ojima, I., 2010. Mechanism-based tumor-targeting drug delivery system: validation of efficient vitamin receptor-mediated endocytosis and drug release. *Bioconjug. Chem.* 21, 979–987.
- Conte, C., d'Angelo, I., Miro, A., Ungaro, F., Quaglia, F., 2014. PEGylated polyester-based nanocapsules. *Curr. Top. Med. Chem.* 14, 1097–1114.
- Costabile, G., d'Angelo, I., Rampioni, G., Bondi, R., Pompili, B., Ascenzioni, F., Mitidieri, E., d'Emmanuele d. V., Sorrentino, R., Miro, A., Quaglia, F., Imperi, F., Leoni, L., Ungaro, F., 2015. Toward repositioning niclosamide for antiviral therapy of *Pseudomonas aeruginosa* lung infections: development of inhalable formulations through nanosuspension technology. *Mol. Pharm.* 12, 2604–2617.
- De Filippis, D., Russo, A., De Stefano, D., Cipriano, M., Esposito, D., Grassia, G., Carnuccio, R., Russo, G., Iuvone, T., 2016. Palmitoylethanolamide inhibits mCP-5 expression by regulating MITF activation in rat chronic granulomatous inflammation. *Eur. J. Pharmacol.* 725, 64–69.
- Ding, H., Yong, K.T., Law, W.C., Roy, I., Hu, R., Wu, F., Zhao, W., Huang, K., Erogbogbo, F., Bergey, E.J., Prasad, P.N., 2011. Non-invasive tumor detection in small animals using novel functional Pluronic nanomicelles conjugated with anti-mesothelin antibody. *Nanoscale* 3, 1813–1822.
- Eckford, P.D., Sharom, F.J., 2009. ABC efflux pump-based resistance to chemotherapy drugs. *Chem. Rev.* 109, 2989–3011.
- Esposito, D., Crescenzi, E., Sagar, V., Loreni, F., Russo, A., Russo, G., 2014. 2014: human rpl3 plays a crucial role in cell response to nucleolar stress induced by 5-FU and L-OHP. *Oncotarget* 5, 11737–11751.
- Heo, D.N., Yang, D.H., Moon, H.J., Lee, J.B., Bae, M.S., Lee, S.C., Lee, W.J., Sun, I.C., Kwon, I.K., 2012. Gold nanoparticles surface-functionalized with paclitaxel drug and biotin receptor as theranostic agents for cancer therapy. *Biomaterials* 33, 856–866.
- Jung, Y.W., Lee, H., Kim, J.Y., Koo, E.J., Oh, K.S., Yuk, S.H., 2013. Pluronic-based core/shell nanoparticles for drug delivery and diagnosis. *Curr. Med. Chem.* 20, 3488–3499.
- Jung, D., Maiti, S., Lee, J.H., Lee, J.H., Kim, J.S., 2014. Rational design of biotin-disulfide-coumarin conjugates: a cancer targeted thiol probe and bioimaging. *Chem. Commun. (Camb.)* 50, 3044–3047.
- Kabanov, A.V., Batrakova, E.V., Alakhov, V.Y., 2002. Pluronic block copolymers as novel polymer therapeutics for drug and gene delivery. *J. Control Release* 82, 189–212.
- Kalyanasundaram, K., Thomas, J.K., 1977. Environmental effects on vibronic band intensities in pyrene monomer fluorescence and their application in studies of micellar systems. *J. Am. Chem. Soc.* 99, 2039–2044.
- Li, Z.L., Xiong, X.Y., Li, Y.P., Gong, Y.C., Gui, X.X., Ou-Yang, X., Lin, H.S., Zhu, L.J., Xie, J.L., 2010. Synthesis and self-assembling behaviors of biotinylated pluronic/poly(lactic acid) biocompatible block copolymers in aqueous solutions. *J. Appl. Polym. Sci.* 115, 1573–1580.
- Li, R., Hu, Z., Sun, S.Y., Chen, Z.G., Owonikoko, T.K., Sica, G.L., Ramalingam, S.S., Curran, W.J., Khuri, F.R., Deng, X., 2013. Niclosamide overcomes acquired resistance to erlotinib through suppression of STAT3 in non-small cell lung cancer. *Mol. Cancer Ther.* 12, 2200–2212.
- Li, Y., Li, P.K., Roberts, M.J., Arend, R.C., Samant, R.S., Buchsbaum, D.J., 2014. Multi-targeted therapy of cancer by niclosamide: a new application for an old drug. *Cancer Lett.* 349, 8–14.
- Liu, C., Lou, W., Zhu, Y., Nadiminty, N., Schwartz, C.T., Evans, C.P., Gao, A.C., 2014. Niclosamide inhibits androgen receptor variants expression and overcomes enzalutamide resistance in castration-resistant prostate cancer. *Clin. Cancer Res.* 20, 3198–3210.
- Liu, C., Lou, W., Armstrong, C., Zhu, Y., Evans, C.P., Gao, A.C., 2015. Niclosamide suppresses cell migration and invasion in enzalutamide resistant prostate cancer cells via Stat3-AR axis inhibition. *Prostate* 75, 1341–1353.
- Maiolino, S., Russo, A., Pagliara, V., Conte, C., Ungaro, F., Russo, G., Quaglia, F., 2015. Biodegradable nanoparticles sequentially decorated with Polyethyleneimine

- and Hyaluronan for the targeted delivery of docetaxel to airway cancer cells. *J. Nanobiotechnol.* 13, 29.
- Maiti, S., Park, N., Han, J.H., Jeon, H.M., Lee, J.H., Bhuniya, S., Kang, C., Kim, J.S., 2013. Gemcitabine-coumarin-biotin conjugates: a target specific theranostic anticancer prodrug. *J. Am. Chem. Soc.* 135, 4567–4572.
- Milone, M.R., Pucci, B., Bruzzese, F., Carbone, C., Piro, G., Costantini, S., Capone, F., Leone, A., Di Gennaro, E., Caraglia, M., Budillon, A., 2013. Acquired resistance to zoledronic acid and the parallel acquisition of an aggressive phenotype are mediated by p38-MAP kinase activation in prostate cancer cells. *Cell. Death Dis.* 4, e641.
- Morral-Ruiz, G., Melgar-Lesmes, P., Lopez-Vicente, A., Solans, C., Garcia-Celma, M., 2015. Biotinylated polyurethane-urea nanoparticles for targeted theranostics in human hepatocellular carcinoma. *Nano Res.* 8, 1729–1745.
- Novac, N., 2013. Challenges and opportunities of drug repositioning. *Trends Pharmacol. Sci.* 34, 267–272.
- Pelosi, D.S., Tessaro, A.L., Moret, F., Gaio, E., Reddi, E., Caetano, W., Quaglia, F., Hioka, N., 2016. Pluronic- κ mixed micelles as efficient nanocarriers for benzoporphyrin derivatives applied to photodynamic therapy in cancer cells. *J. Photochem. Photobiol. A: Chem.* 314, 143–154.
- Pagliara, V., Saide, A., Mitidieri, E., d'Emmanuele di Villa Bianca, R., Sorrentino, R., Russo, G., 2016. 5-FU targets rp to induce mitochondrial apoptosis via cystathionine- β -synthase in colon cancer cells lacking p53. *Oncotarget* doi: <http://dx.doi.org/10.18632/oncotarget.10385>.
- Rabik, C.A., Dolan, M.E., 2007. Molecular mechanisms of resistance and toxicity associated with platinating agents. *Cancer Treat. Rev.* 33, 9–23.
- Ren, X., Duan, L., He, Q., Zhang, Z., Zhou, Y., Wu, D., Pan, J., Pei, D., Ding, K., 2010. Identification of niclosamide as a new small-molecule inhibitor of the STAT3 signaling pathway. *ACS Med. Chem. Lett.* 1, 454–459.
- Russo, A., Siciliano, G., Catillo, M., Giangrande, C., Amoresano, A., Pucci, P., Pietropaolo, C., Russo, G., 2010. hnRNP H1 and intronic G runs in the splicing control of the human rpl3 gene. *Biochim. Biophys. Acta* 1799, 419–428.
- Russo, A., Catillo, M., Esposito, D., Briata, P., Pietropaolo, C., Russo, G., 2011. Autoregulatory circuit of human rpl3 expression requires hnRNP H1 NPM and KHSRP. *Nucleic Acids Res.* 39, 7576–7585.
- Russo, A., Pagliara, V., Albano, F., Esposito, D., Sagar, V., Loreni, F., Irace, C., Santamaria, R., Russo, G., 2016. Regulatory role of rpl3 in cell response to nucleolar stress induced by Act D in tumor cells lacking functional p53. *Cell Cycle* 15, 41–51.
- Sack, U., Walther, W., Scudiero, D., Selby, M., Kobelt, D., Lemm, M., Fichtner, I., Schlag, P.M., Shoemaker, R.H., Stein, U., 2011. Novel effect of antihelminthic niclosamide on S100A4-mediated metastatic progression in colon cancer. *J. Natl. Cancer Inst.* 103, 1018–1036.
- Schinkel, A.H., Jonker, J.W., 2003. Mammalian drug efflux transporters of the ATP binding cassette (ABC) family: an overview. *Adv. Drug Deliv. Rev.* 55, 3–29.
- Shim, J.S., Liu, J.O., 2014. Recent advances in drug repositioning for the discovery of new anticancer drugs. *Int. J. Biol. Sci.* 10, 654–663.
- Siegel, R.L., Miller, K.D., Jemal, A., 2015. Cancer statistics, 2015. *CA Cancer J. Clin.* 65, 5–29.
- Staud, F., Pavek, P., 2005. Breast cancer resistance protein (BCRP/ABCG2). *Int. J. Biochem. Cell Biol.* 37, 720–725.
- Stenvang, J., Kumler, I., Nygard, S.B., Smith, D.H., Nielsen, D., Brunner, N., Moreira, J. M., 2013. Biomarker-guided repurposing of chemotherapeutic drugs for cancer therapy: a novel strategy in drug development. *Front. Oncol.* 3, 313.
- Strouse, J.J., Ivitski-Steele, I., Waller, A., Young, S.M., Perez, D., Evangelisti, A.M., Ursu, O., Bologna, C.G., Carter, M.B., Salas, V.M., Tegos, G., Larson, R.S., Oprea, T.I., Edwards, B.S., Sklar, L.A., 2013. Fluorescent substrates for flow cytometric evaluation of efflux inhibition in ABCB1 ABCC1, and ABCG2 transporters. *Anal. Biochem.* 437, 77–87.
- Stylianopoulos, T., Jain, R.K., 2015. Design considerations for nanotherapeutics in oncology. *Nanomedicine* 11, 1893–1907.
- Wang, W., Ke, S., Chen, G., Gao, Q., Wu, S., Wang, S., Zhou, J., Yang, X., Lu, Y., Ma, D., 2004. Effect of lung resistance-related protein on the resistance to cisplatin in human ovarian cancer cell lines. *Oncol. Rep.* 12, 1365–1370.
- Wang, Y., Zhou, K., Huang, G., Hensley, C., Huang, X., Ma, X., Zhao, T., Sumer, B.D., DeBerardinis, R.J., Gao, J., 2014. A nanoparticle-based strategy for the imaging of a broad range of tumours by nonlinear amplification of microenvironment signals. *Nat. Mater.* 13, 204–212.
- Xiang, D., Yuan, Y., Chen, L., Liu, X., Belani, C., Cheng, H., 2015. Niclosamide an anti-helminthic molecule, downregulates the retroviral oncoprotein Tax and pro-survival Bcl-2 proteins in HTLV-1-transformed T lymphocytes. *Biochem. Biophys. Res. Commun.* 464, 221–228.
- Zhang, X., Jackson, J.K., Burt, H.M., 1996. Determination of surfactant critical micelle concentration by a novel fluorescence depolarization technique. *J. Biochem. Biophys. Methods* 31, 145–150.
- Zhang, W., Shi, Y., Chen, Y., Ye, J., Sha, X., Fang, X., 2011. Multifunctional Pluronic P123/F127 mixed polymeric micelles loaded with paclitaxel for the treatment of multidrug resistant tumors. *Biomaterials* 32, 2894–2906.
- Zhu, P., Zhao, N., Sheng, D., Hou, J., Hao, C., Yang, X., Zhu, B., Zhang, S., Han, Z., Wei, L., Zhang, L., 2016. Inhibition of growth and metastasis of colon cancer by delivering 5-fluorouracil-loaded pluronic P85 copolymer micelles. *Sci. Rep.* 6, 20896.
- d'Angelo, I., Conte, C., Miro, A., Quaglia, F., Ungaro, F., 2014. Core-shell nanocarriers for cancer therapy: part I: biologically oriented design rules. *Expert Opin. Drug Deliv.* 11, 283–297.
- d'Emmanuele, V.d., Mitidieri, E., Esposito, D., Donnarumma, E., Russo, A., Fusco, F., Ianaro, A., Mirone, V., Cirino, G., Russo, G., Sorrentino, R., 2015. Human cystathionine-beta-synthase phosphorylation on serine227 modulates hydrogen sulfide production in human urothelium. *PLoS One* 10, e0136859.